RSC Advances

PAPER

View Article Online
View Journal | View Issue

Cite this: *RSC Adv.*, 2020, **10**, 37500

Tb(III)-doped nanosheets as a fluorescent probe for the detection of dipicolinic acid

Bing Wang,[a] Jinfeng Xia,[b] Guohong Zhou,[b] Xin Li,[a] Mengting Dai,[a] Danyu Jiang[b] and Qiang Li *[a]

A new fluorescent probe based on terbium(III)-doped nanosheets was designed for detecting low-levels of dipicolinic acid (DPA), a biomarker of bacterial spores. The ability to detect ultra-low concentrations of DPA is therefore of great significance. First, Tb(III)-doped ytterbium hydroxide nanosheets were obtained by mechanical exfoliation from layered rare-earth hydroxide (LRH) materials. The morphology of the as-synthesized nanosheets was studied by transmission electron microscopy and atomic force microscopy. The Tb(III)-doped nanosheets are demonstrated to be highly sensitive to DPA, which remarkably enhances Tb(III) luminescence intensities at a wavelength of 544 nm. Furthermore, Tb(III) emission increases linearly with DPA concentration. Selectivity studies were conducted by adding different competing aromatic ligands to the sensing solution; however, their fluorescence responses were observed to be negligibly small in comparison with that of DPA. Our findings provide a basis for the application of Tb(III)-doped nanosheets for accurate, sensitive, and selective monitoring of DPA as a biomarker of anthrax.

Received 20th November 2019
Accepted 1st October 2020

DOI: 10.1039/c9ra09695g

rsc.li/rsc-advances

Introduction

Anthrax is an acute infectious disease caused by *Bacillus anthracis*, which is a serious threat to human health.[1–3] Because of the known high incidence and mortality rate, *Bacillus anthracis* spores have been employed as one of the most potentially destructive biological warfare agents.[4–6] Dipicolinic acid, which is a major component of many pathogenic bacterial spores (5–15% of dry mass)[7–10] such as *Bacillus anthracis* and *Bacillus subtilis*, is not a component of other commonly occurring bacteria. Furthermore, the mortality rate of anthrax caused by *Bacillus anthracis* is very high, and according to many literature sources, DPA can be used as a biomarker of *Bacillus anthracis*.[11–14] Therefore, a method for the efficient, rapid, and sensitive quantitative detection of DPA would have enormous practical significance.

Due to special monolayer structure of yttrium hydroxide nanosheets, doped Eu^{3+} or Tb^{3+} as luminescence centers completely exposure to the environment. So the luminescent properties of Eu^{3+} or Tb^{3+} doped yttrium hydroxide nanosheets are very sensitive to the environment. Therefore a high sensitivity luminescent probe can be designed based on Eu^{3+} or Tb^{3+} doped yttrium hydroxide nanosheets. Owing to its advantages of high sensitivity, good selectivity, and short response times, the use of fluorescence as a detection method has increasingly attracted the attention of researchers.[15–18] DPA is sensitive to the luminescence of trivalent europium and terbium ions, thanks to matching energy levels, and the luminescence intensity is related to the concentration of DPA.[7,19] Lanthanide ions have intrinsically weak fluorescence emission because the emission arises from forbidden f–f electron transitions. The ligand-containing chromophore (antenna) coordinates with lanthanide ions, and the triplet excited state of the ligand transfers energy to the emission state of the lanthanide ions to enhance lanthanide luminescence. The phenomenon is called the antenna effect. According to Scheme 1, after coordination with the trivalent terbium ion, DPA can sensitize Tb(III) upon excitation by ultraviolet (UV) light, and the fluorescence intensity is greatly increased by the absorption-energy transfer-emission process.[20–22] Based on the above characteristics, the use of the Tb(III) ion has become one of the most popular approaches to detect DPA, with extremely high sensitivity as well as accurate and reliable detection results.[11]

Nano-structured materials have special surface and interface effects and are advantageous because of their small size, and therefore, they are excellent candidates for the preparation of biochemical probes.[23,24] Therefore, many types of fluorescent probes based on nanostructured materials have been developed. For example, Tan *et al.* prepared a nanosized coordination polymer based on rare-earth nucleotides (Tb adenosine monophosphate AMP) and developed silver nanoparticles based on terbium-ion functionalization for the detection of DPA.[9,25] In addition, Xu *et al.* prepared fluorapatite nanocrystals

[a]*School of Chemistry and Molecular Engineering, East China Normal University, Shanghai 200062, P. R. China. E-mail: qli@chem.ecnu.edu.cn*
[b]*Shanghai Institute of Ceramics, Chinese Academy of Sciences, Shanghai 200050, P. R. China*

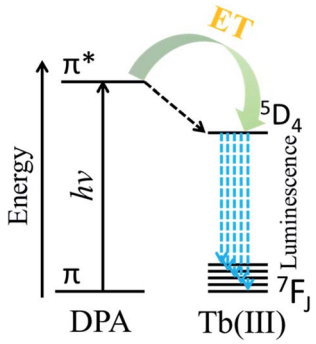

Scheme 1 Antenna effect of the DPA ligand on Tb(III).

doped with the rare-earth ions europium and terbium for the detection of bacterial spores using the biomarker DPA.[11]

As described in our previous paper, nanosheets, which possess unique chemical and physical properties owing to their excellent two-dimensional anisotropy, show enhanced luminescence compared with Tb(III) complexes. Furthermore, such nanosheets can be used to prepare highly responsive fluorescent sensors. As reported previously, sensors based on Eu(III) or Tb(III)-doped nanosheets can sensitively and reliably detect bilirubin in human serum samples[26,27] and in dissolved or gaseous oxygen.[28]

These advantageous properties motivated us to develop a novel fluorescence probe based on nanosheets doped with 1% Tb(III) ions, as reported in this paper, to be used for the detection of *Bacillus anthracis* with high sensitivity and selectivity. The energy transferred during the coordination interaction between DPA and the terbium ion linearly enhances the fluorescence of the nanosheets. Thus, a fluorescent probe consisting of Tb(III)-doped nanosheets for the detection of *Bacillus anthracis* can achieve a detection limit as low as 44 nmol L^{-1} and, in addition, it exhibits good selectivity for DPA with respect to potential interferences from aromatic ligands and selected amino acids.

Materials and methods

Chemicals, reagents, and apparatus

The following chemicals of analytical purity were obtained from J&K Chemicals and were used directly without further purification: yttrium oxide (Y_2O_3), terbium oxide (Tb_4O_7), concentrated nitric acid, sodium benzoate, ethanol, pyridine-2,6-dicarboxylic acid (DPA), benzoic acid (BA), *o*-dibenzoic acid (*o*-PA), *m*-dibenzoic acid (*m*-PA), *p*-dibenzoic acid (*p*-PA), trimesic acid (TMA), glycine (Gly), D-aspartic acid (ASP), and the peptide glutathione (GSH). Luminescence spectra were recorded on a FLS-980 spectrofluorometer (Edinburgh Instruments, UK) equipped with a quartz cuvette (1.0 cm × 1.0 cm) using 1 nm slit widths for excitation and emission. UV-vis absorption spectra were recorded using an Agilent Cary UV-8000 spectrophotometer (Tianmei, China).

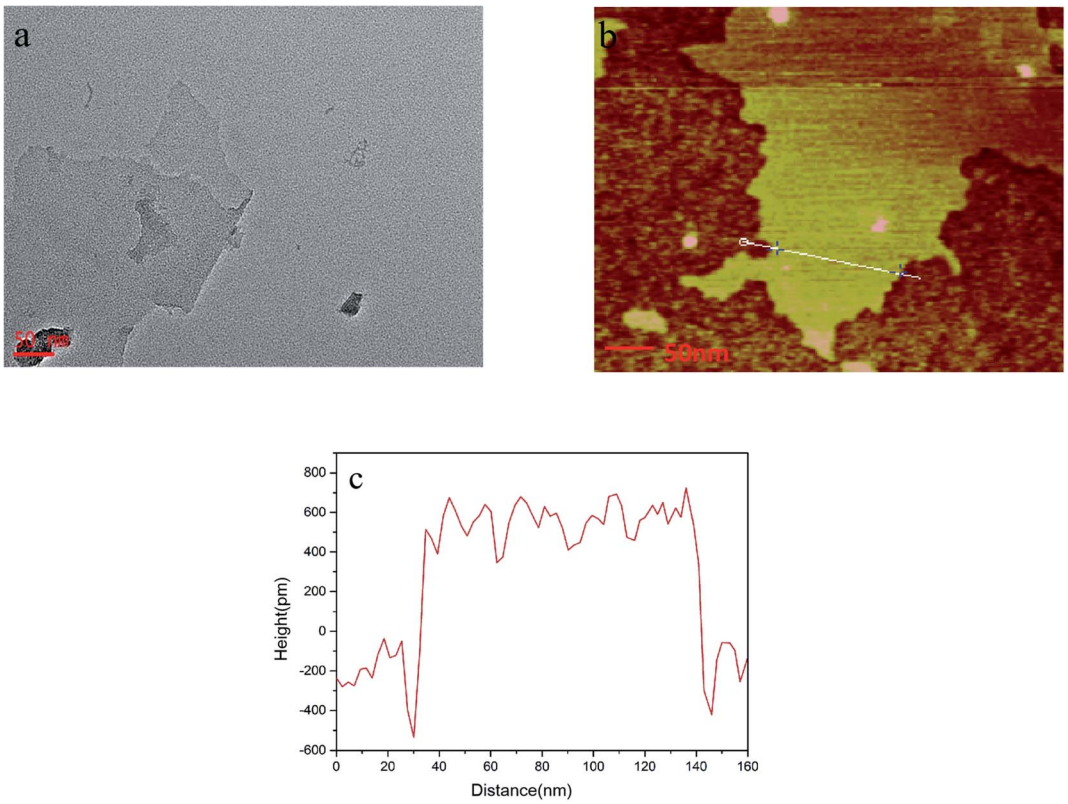

Fig. 1 (a) Transmission electron microscopy (TEM) image of nanosheets. (b) Atomic force microscopy (AFM) images of nanosheets and (c) cross-sectional AFM image illustrating the nanosheet thickness.

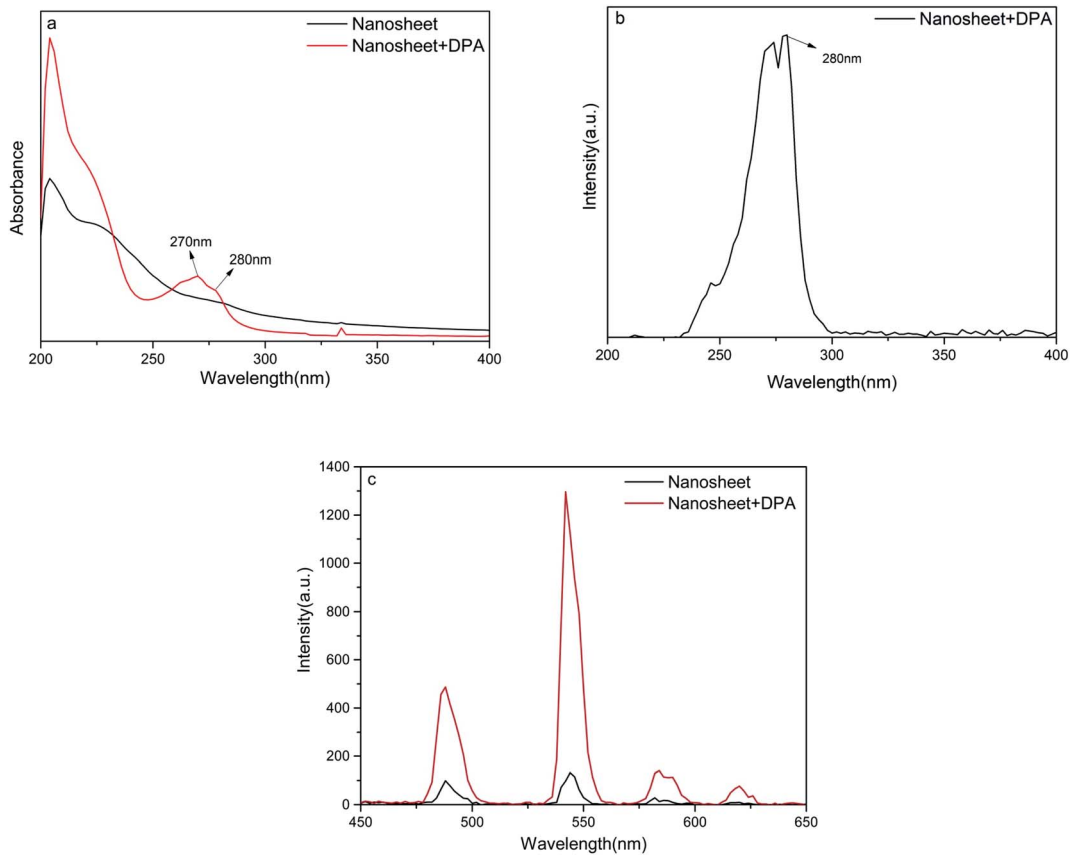

Fig. 2 (a) UV absorption spectra before and after the addition of DPA to nanosheets. (b) Excitation spectra after adding DPA to nanosheets. (c) Emission spectra before and after the addition of DPA to nanosheets.

Synthesis of Tb(III)-doped nanosheets

Layered yttrium hydroxides doped with 1% Tb(III) were synthesized according to our previously described method,[29] which is highly efficient and inexpensive. Ultra-thin nanosheets were prepared by ultrasonic dispersion of 0.1 g of the as-received layer compound in 200 mL of ethanol. The dispersed solution was placed in a centrifuge (4000 rpm), and a nanosheet sol was obtained after separation. The concentration of terbium ions in the nanosheet sol was 46.7 μmol L^{-1}, as determined by titration.

Detection of DPA

DPA detection was conducted as follows: 100 μL of the nanosheet sol was mixed with different volumes of a DPA solution in ethanol (100 μmol L^{-1}), and this was further diluted to obtain a volume of 2000 μL with ethanol solvent. Then, specimens with different concentrations of DPA (0–30 μmol L^{-1}) were prepared. The pH value of the solution was approximately 7. The effect of different DPA concentrations on the fluorescence intensity at the optimal emission wavelength for trivalent terbium ions, 544 nm, was recorded (λ_{ex} = 280 nm).

Results and discussion

Characterization of nanosheets

The morphology of the layered nanosheets was observed by acquiring images using transmission electron microscopy (TEM) (Fig. 1a) and atomic force microscopy (AFM) (Fig. 1b). The lateral dimension of the nanosheets spans approximately several hundred nanometers, and the thickness of the nanosheets, as measured using Fig. 1c is approximately 1 nm, which means that single-layer nanosheets were obtained.

The spectral properties of the as-prepared nanosheets were studied. First, the UV absorption spectra of the as-prepared nanosheet sol was recorded before and after the addition of DPA, using a UV-vis spectrometer (UV-8000, Metash). These spectroscopic results are similar to those reported by other researchers.[30–32] In Fig. 2a, the bands in the region of 190–240 nm are assigned to the π–π* transition of an aromatic pyridine ring or to a π_{ring}–π_{CO} transition. The bands at 270 and 280 nm in the UV absorption spectra belong to the CT transition (charge transfer state); electrons that occupy the highest MO orbital are transferred from one carbonyl to another through the pyridine nucleus. The transition resulting in the band at 280 nm involves two oxygen atoms and a nitrogen atom that coordinate with the Tb(III) ion. Therefore, the 280 nm band might be a suitable excitation wavelength. Furthermore, the fluorescence excitation spectra (Fig. 2b) confirm that an excitation wavelength of 280 nm is the most effective. The fluorescence intensity of the nanosheets increases obviously after the addition of DPA (Fig. 2c), indicating that our nanosheets are responsive to DPA.

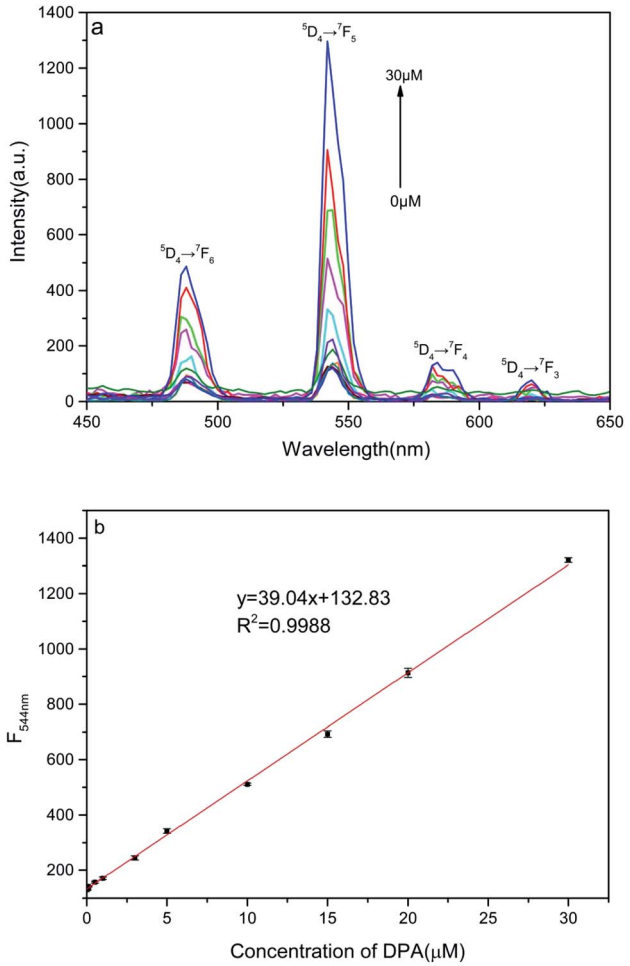

Fig. 3 (a) Fluorescence spectra of Tb(III) ion–DPA complexes in solution for various DPA concentrations. (b) Linear relation between fluorescence intensity at 544 nm and DPA concentration.

Response of nanosheet fluorescent probe to DPA

An increase in the DPA concentration caused the fluorescence intensity of the four characteristic peaks of the terbium ion located at 488 nm ($^5D_4 \rightarrow {}^7F_6$), 544 nm ($^5D_4 \rightarrow {}^7F_5$), 584 nm ($^5D_4 \rightarrow {}^7F_4$), and 620 nm ($^5D_4 \rightarrow {}^7F_3$) to increase, as monitored at an excitation wavelength of 280 nm. As shown in Fig. 3a and b, the fluorescence intensity of the strongest emission peak, at 544 nm, $I_{544\ nm}$, increases linearly with DPA concentration in the range of 50 nmol L^{-1} to 30 μmol L^{-1}. The linear equation for this relationship is $y = 39.4x + 132.8$ and the correlation coefficient is 0.9988. Hence, the signal-to-noise ratio is 3, and the calculated limit of detection for this method is 44 nmol L^{-1}, which is much lower than a minimum for human beings of 10^4 spores per milliliter (about 0.1 μM of DPA).[9,14,33,34] These results indicate that the nanosheet probe prepared by us is highly suitable for the detection of DPA.

The sensing materials and correlation coefficient used in recent years for detecting DPA (summarized in Table 1) were essentially all one-dimensional nanoparticles, quantum dots, and MOFs. In the case of nanoparticles, rare-earth ions need to be exposed on the surface of these particles to enable them to coordinate with DPA. However, in our as-synthesized two-dimensional nanosheets, all the rare-earth ions are directly exposed on the exterior surfaces where they are able to efficiently interact with DPA. This explains the low detection limit of the nanosheet fluorescent probe (44 nmol L^{-1}) and the relatively large detection range (0–30 μmol L^{-1}), linear correlation coefficient of 0.9988. In addition, the nanosheet fluorescent probe is convenient to use and inexpensive because of the simple fabrication method.

Selectivity is another important parameter for the design of probes. It could be known from references that when rare earth ions were tested for DPA in a physical environment, it might be affected by many factors. For example, inorganic salts, organic substances, amino acids, through reading the literature, most inorganic salts will not affect the luminescence of rare earth ions, so we did not choose some common inorganic salts for experiments. The selectivity of the nanosheet fluorescent probe was verified by investigating several potentially interfering aromatic organic molecules. When the DPA is detected by a fluorescent probe, the measurement signal may be affected by a variety of factors. According to some ref. 9, 11, 15, 40 and 42, some aromatic ligands with structures similar to DPA may also coordinate with Tb(III) and affect luminescence. Therefore, several representative aromatic ligands were selected for the interference experiments. In addition, considering the coordination of nitrogen with Tb(III) and that there may also be benzene rings in some amino acids, several amino acids were also selected for the interference experiments. The selected ligands were benzoic acid (BA), *o*-dibenzoic acid (*o*-PA), *m*-dibenzoic acid (*m*-PA), *p*-dibenzoic acid (*p*-PA), trimesic acid (TMA), and several amino acids, such as glycine (Gly), D-aspartic

Table 1 Performance comparison for various types of sensing materials employed for the detection of DPA

Sensing material	Linear range (μmol L^{-1})	Detection limit (nmol L^{-1})	Correlation coefficient	Ref.
Luminescent (MOF)	0–120	4500	0.992	13
Eriochrome complex	0–32	2000	—	35
Luminescent (MOF)	0–120	3200	0.998	36
Quantum dots	0–34	1020	0.997	37
Micelle	0–7	54	0.999	15
Flexible polymer-film	0–50	100	0.989	38
Nanoparticles	—	48	0.994	39
Nanosheets	0–30	44	0.9988	This work

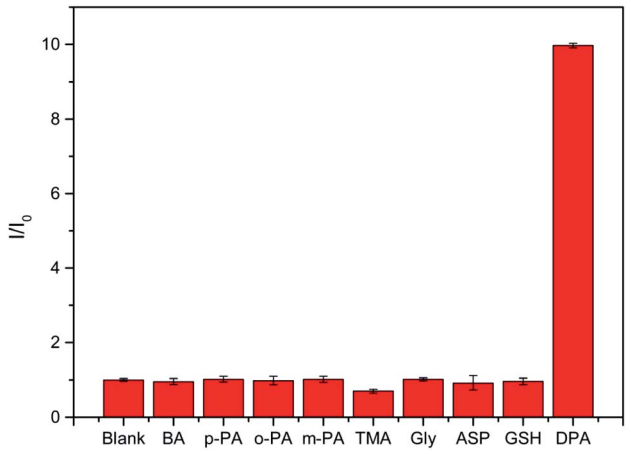

Fig. 4 Response of nanosheet fluorescent probe to 100 μmol L^{-1} of various potentially interfering organic molecules compared with 30 μmol L^{-1} of DPA.

acid (ASP), glutathione peptide (GSH), were also tested. As shown in Fig. 4, the nanosheet fluorescent probe only responded slightly to the selected organic molecules at concentrations of 100 μmol L^{-1}, whereas 30 μmol L^{-1} of DPA caused the nanosheet fluorescent probe to exhibit strong emission. These results confirm the high selectivity of the nanosheet fluorescent probes for the detection of DPA.

Sensing mechanism of nanosheet probe

Fourier-transform infrared (FT-IR) spectroscopy was employed to study the structural changes and interactions after DPA was added to the nanosheet sol. As shown in Fig. 5, three characteristic peaks appear in the FT-IR spectrum of the nanosheets before the addition of DPA (black line). The first is the broad peak at 3432 cm^{-1}, caused by water molecules absorbed on the nanosheets. The next peak, observed at 1598 cm^{-1}, can be attributed to the C–C stretching vibration in benzene, whereas the other two peaks, at 1542 and 1419 cm^{-1}, can be attributed to

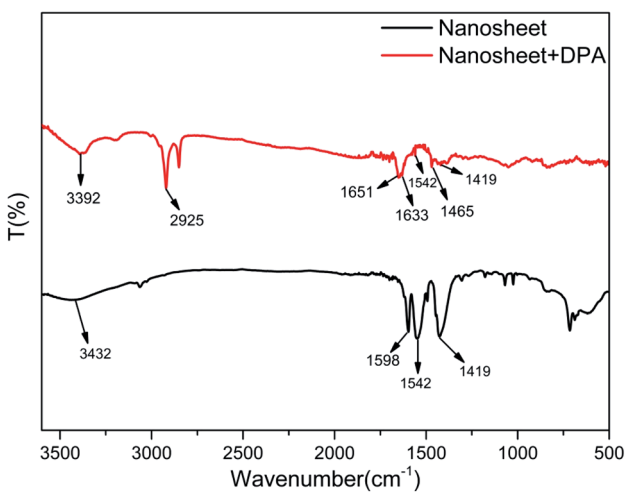

Fig. 5 FT-IR spectra before and after addition of DPA to nanosheets.

the chelation between the benzoate and the rare-earth ions.[27] The changes in the FT-IR spectrum after the addition of DPA (red spectrum, Fig. 5) are as follows: the peak at 3432 cm^{-1} resulting from water disappears, and the peaks ascribed to benzoate are noticeably attenuated. In addition, some new peaks appear. The peak at 3392 cm^{-1} is the –OH stretching vibration band of the hydroxide units in the nanosheet framework, and that at 2925 cm^{-1} is assigned to the C–H absorption of the pyridine ring of DPA. The three other peaks, which are also assigned to DPA, are the peak at 1651 cm^{-1} resulting from the C=O double bond of the carboxyl group of DPA, and those at 1633 cm^{-1} and 1465 cm^{-1}, which are respectively assigned to the C=N and C=C double bonds of the DPA pyridine ring. However, the bands at 1651 and 1633 cm^{-1} are redshifted compared with the pure DPA peaks.[43] This phenomenon can be explained by taking into consideration the coordination of DPA with the rare-earth ions on the nanosheets. Furthermore, DPA complexes with rare earth ions replaces water molecules and benzoate ions on the nanosheets, thereby weakening the water IR absorption and resulting in the disappearance of the associated peaks from the FT-IR spectrum.

The overall mechanism of DPA detection by the nanosheet fluorescent probe is illustrated in Fig. 6. Before the addition of DPA, all the rare-earth ions, including the fluorescent Tb(III) center, on the nanosheets are completely coordinated to benzoate ions and water molecules. In the form in which it is coordinated to water, Tb(III) is known to exhibit low-intensity fluorescence, owing to nonradiative quenching resulting from the strong vibronic coupling of water molecules. Once DPA is added, it gradually replaces the water molecules and benzoate ions, and strongly coordinates with the rare-earth ions on the nanosheets. Because the lowest triplet energy level of DPA matches the emission state energy of Tb(III), energy transfer from DPA to the fluorescent center of Tb(III)[37] is realized, and the fluorescence intensity of Tb(III) is greatly improved owing to the antenna effect of the DPA ligand. Thanks to the replacement of water molecules and the antenna effect, the nanosheet fluorescent probe is highly sensitive to DPA. Thus, the ability to detect ultra-low concentrations of DPA is highly significant because of the unique single-layer two-dimensional structure of the nanosheets, in which DPA can strongly coordinate with each of the Tb(III) ions inserted in stable nanosheets and act as an efficient antenna for the fluorescent center. Therefore, it is thought that nanosheets with a single layer should possess better structures for use as fluorescent probes with respect to conventional nanoparticle structures. Thus, the nanosheet fluorescent probe is a potentially highly sensitive and selective detector of the anthrax biomarker DPA.

The interaction between the nanosheet fluorescent probe and DPA was also studied by measuring the fluorescence lifetime of the nanosheets before and after adding DPA. The fluorescence decay curves in Fig. 7 indicate that the fluorescence lifetime increases with DPA concentration. A double exponential function (eqn (1)) was employed to fit the fluorescence decay curves, and the resulting fit parameters are listed in Table 2.

$$I = A_1 \exp(-t/\tau_1) + A_2 \exp(-t/\tau_2) \quad (1)$$

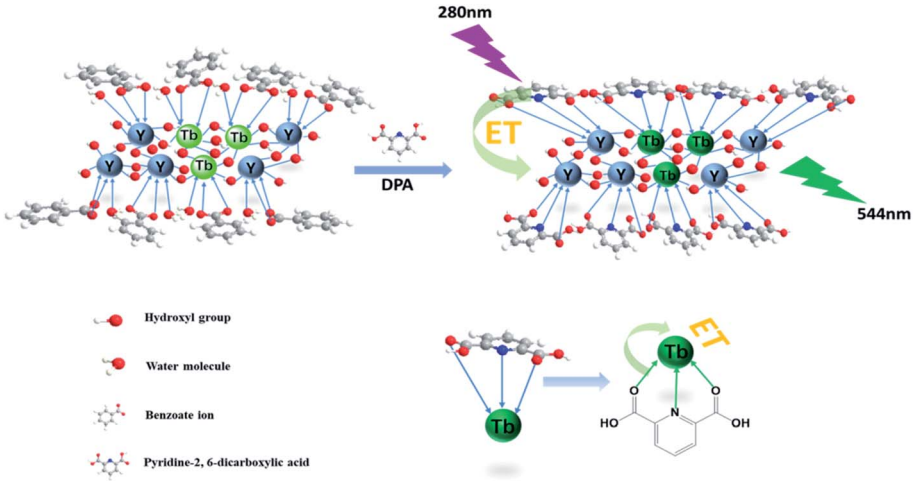

Fig. 6 Schematic diagram of the mechanism of the nanosheet fluorescent probe for DPA detection.

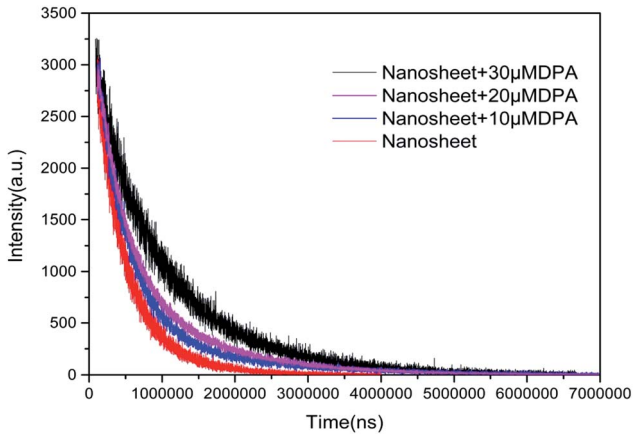

Fig. 7 Fluorescence intensity as a function of time after the addition of different concentration DPA to nanosheets.

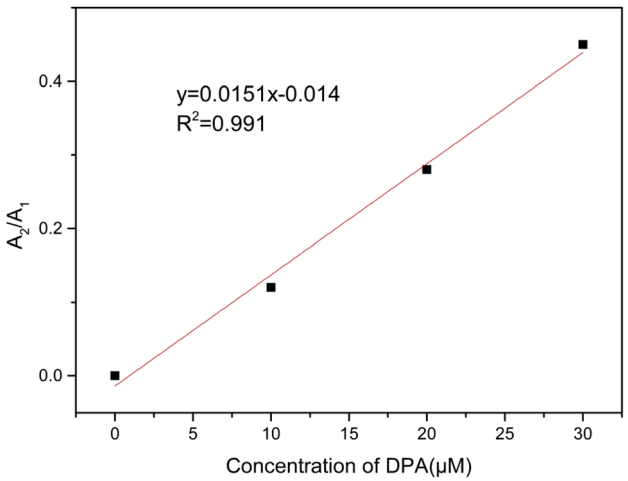

Fig. 8 Linear relation between A_2/A_1 and DPA concentration.

When there is no DPA, the fluorescence decay curve of the Tb(III)-doped nanosheets coordinated with water fits a single-exponential curve with a short lifetime (τ_1 = 418 μs). After DPA was added, coordinating with Tb(III), the fluorescence decay curve fit the double exponential expression well, including fast processes (τ_1, 357, 381 and 423 μs) and slow processes (τ_2, 1070, 1193 and 1758 μs). The observed fast lifetimes, those close to that of the probe without DPA, can still originate from Tb(III) coordinated with water. It was reported[6,23] that the decrease in the coordination sites of water molecules after the addition of DPA reduced the non-radiative quenching effect of water molecules on Tb(III), thus prolonging the fluorescence lifetime and enhancing fluorescence intensity. Therefore, the slow process can be attributed to Tb(III) coordinated by DPA. Furthermore, when the concentration of DPA rises and more DPA replaces water molecules to coordinate with Tb(III), increasing of the mean lifetime, the ratio of A_2/A_1 also increased and showed a linear correlation with the concentration of DPA (as shown in Fig. 8). The behavior of the fluorescence decay is agreement with our above-described proposed mechanism.

Table 2 Fluorescence decay lifetime parameters

Concentration (μM)	A_1	τ_1 (μs)	A_2	τ_2 (μs)	R^2
0	2443	418	—	—	0.994
10	2253	423	278	1758	0.997
20	2629	357	733	1070	0.991
30	1726	381	783	1193	0.999

Conclusions

In summary, in this paper, we reported the use of a nanosheet sol doped with Tb(III), synthesized by ultrasonic exfoliation from layered yttrium hydroxide compounds, for the design of a new fluorescent probe to detect DPA, a biomarker for bacterial spores. Because of the unique single-layer two-dimensional

structure of the nanosheets, DPA is able to displace the water molecules, strongly coordinate with each of the Tb(III) ions inserted into the stable nanosheets, and act as an efficient antenna of the fluorescent center. As a result, the fluorescence intensity of the nanosheets increases linearly with DPA concentration. This fluorescent probe exhibits a large detection range of 0–30 μmol L^{-1} DPA, a low detection limit of 44 nmol L^{-1}, and good selectivity. This highly sensitive and low-cost fluorescent probe based on nanosheets is a promising candidate for the detection of DPA.

Conflicts of interest

The authors declare that they have no conflict of interest.

Acknowledgements

This research did not receive any specific grant from funding agencies in the public, commercial, or not-for-profit sectors.

References

1 P. D. Filippo, D. Pomata, C. Riccardi, F. Buiarelli, *et al.*, *Anal. Bioanal. Chem.*, 2017, **409**, 1657–1666.
2 M. Cho, S. Chung, J. H. Jung, G. E. Rhie, J. H. Jeon and T. S. Seo, *Biosens. Bioelectron.*, 2014, **61**, 172–176.
3 M. K. Sharma, J. Narayanan, D. Pardasani, D. N. Srivastava, S. U. Spadhyay and A. K. Goel, *Biosens. Bioelectron.*, 2016, **80**, 442–449.
4 R. K. Gao, J. H. Ko, K. W. Cha, J. H. Jeon, G. E. Rhie, J. H. Choi, *et al.*, *Biosens. Bioelectron.*, 2015, **72**, 230–236.
5 M. Donmez, H. A. Oktem and M. D. Yilmaz, *Carbohydr. Polym.*, 2018, **180**, 226–230.
6 Y. H. Zhang, B. Li, H. P. Ma, L. M. Zhang and Y. X. Zheng, *Biosens. Bioelectron.*, 2016, **85**, 287–293.
7 Q. X. Wang, S. F. Xue, Z. H. Chen, S. H. Ma, S. Zhang, G. Shi, *et al.*, *Biosens. Bioelectron.*, 2017, **94**, 388–393.
8 M. Rong, Y. Liang, D. Zhao, B. Chen, C. Pan, X. Deng, Y. Chen, *et al.*, *Sens. Actuators, B*, 2018, **265**, 498–505.
9 H. L. Tan, C. J. Ma, L. L. Chen, F. G. Xu, S. H. Chen and L. Wang, *Sens. Actuators, B*, 2014, **190**, 621–626.
10 M. A. Bacigalupo, G. Meroni and R. Longhi, *Talanta*, 2006, **69**, 1106–1111.
11 J. Xu, X. Shen, L. Jia, M. Zhang, T. Zhou and Y. Wei, *Biosens. Bioelectron.*, 2017, **87**, 991–997.
12 N. Bhardwaj, S. Bhardwaj, J. Mehta, K. Kim and A. Deep, *Biosens. Bioelectron.*, 2016, **86**, 799–804.
13 K. Y. Shi, Z. C. Yang, L. H. Dong and B. Yu, *Sens. Actuators, B*, 2018, **266**, 263–269.
14 Y. H. Song, J. Y. Chen, D. Q. Hu, F. F. Liu, P. Li, H. B. Li, *et al.*, *Sens. Actuators, B*, 2015, **221**, 586–592.
15 L. Ke, R. Meng, C. Shan, C. Jing, J. Jia, W. S. Liu and Y. Tang, *Anal. Chem.*, 2018, **90**, 3600–3607.
16 A. S. Maghsoudi, F. Vakhshiteh, R. Torabi, S. Hassani, M. R. Ganjali, P. Norouzi, M. Hosseini and M. Abdollahi, *Biosens. Bioelectron.*, 2018, **99**, 122–135.
17 S. Chen, Y. L. Yu and J. H. Wang, *Anal. Chim. Acta*, 2017, **999**, 13–26.
18 V. S. P. K. Sankara Aditya Jayanthi, A. B. Das and U. Saxena, *Biosens. Bioelectron.*, 2017, **91**, 15–23.
19 W. K. Oh, Y. S. Jeong, J. Song and J. Jiang, *Biosens. Bioelectron.*, 2011, **29**, 172–177.
20 A. Klonkowski, S. Lis, Z. Hnatejko, K. Czarnobaj, M. Pietraszkiewicz and M. Elbanowski, *J. Alloys Compd.*, 2000, **300**, 55–60.
21 Z. Y. Lin, Z. B. Qu, Z. H. Chen, X. Y. Han, L. X. Deng, *et al.*, *Anal. Chem.*, 2019, **91**, 11170–11177.
22 M. C. Rong, X. Z. Deng, S. Chi, L. Z. Huang, Y. B. Zhou, Y. N. Shen and X. Chen, *Microchim. Acta*, 2018, **185**, 2–10.
23 K. Ma, H. Wang, X. Li, B. Xu and W. J. Tian, *Anal. Bioanal. Chem.*, 2015, **407**, 2625–2630.
24 W. Wang, Y. Y. Wang, L. Y. Lin, Y. L. Song, *et al.*, *Anal. Bioanal. Chem.*, 2019, **411**, 4017–4023.
25 H. L. Tan, Q. Li, C. J. Ma, Y. H. Song and F. G. Xu, *J. Nanopart. Res.*, 2014, **16**, 1–11.
26 W. Yang, J. F. Xia, G. H. Zhou, D. Y. Jiang and Q. Li, *RSC Adv.*, 2018, **8**, 17854–17859.
27 W. Yang, Q. Li, X. H. Zheng, X. Li and X. Li, *J. Adv. Ceram.*, 2018, **7**, 352–361.
28 W. Yang, Q. Li, X. H. Zheng, X. Li and X. Li, *Sens. Actuators, B*, 2018, **257**, 340–346.
29 L. Zhang, D. Y. Jiang, J. F. Xia, N. Zhang and Q. Li, *RSC Adv.*, 2014, **34**, 17856–17857.
30 L. Wasylina, E. Kucharska, Z. Weglinski and A. Puszko, *Chem. Heterocycl. Compd.*, 1999, **35**, 210–218.
31 A. G. Viveros-Andrade, R. Colorado-Peralta, M. Flores-Alamo, *et al.*, *J. Mol. Struct.*, 2017, **1145**, 10–17.
32 G. F. Bailey, S. Karp and L. E. Sacks, *J. Bacteriol.*, 1965, **89**, 984–987.
33 D. R. Franz, P. B. Jahrling and A. M. Friedlander, *JAMA*, 1997, **278**, 399–411.
34 D. R. Walt, *Anal. Chem.*, 2000, **72**, 738A–746A.
35 M. D. Yilmaz and H. A. Oktem, *Anal. Chem.*, 2018, **90**, 4221–4225.
36 C. Lin and Z. G. Fang, *Inorg. Chim. Acta*, 2018, **477**, 51–58.
37 H. Chen, Y. J. Xie, A. M. Kirillov, L. L. Liang, M. H. Yu, W. S. Liu and Y. Tang, *Chem. Commun.*, 2015, **51**, 5036–5039.
38 B. L. Ma, F. Zeng and F. Y. Zheng, *Analyst*, 2011, **136**, 3649–3655.
39 W. J. Rieter, K. M. L. Taylor and W. B. Lin, *J. Am. Chem. Soc.*, 2007, **129**, 9852–9853.
40 P. Pellegrino, N. F. Jr, D. Rosen and J. Gillespie, *Anal. Chem.*, 1998, **70**, 1755–1760.
41 A. B. Ammann, L. Kolle and H. Brandl, *Int. J. Microbiol.*, 2011, **2011**, 1–5.
42 Z. Zhou, J. P. Gu, Y. Z. Chen, X. X. Zhang, H. X. Wu and X. G. Qiao, *Spectrochim. Acta, Part A*, 2019, **212**, 88–93.
43 Z. A. Siddiqi, M. Khalid, S. Kumar, M. Shahid and S. Noor, *Eur. J. Med. Chem.*, 2010, **45**, 264–269.

